Mon. Not. R. Astron. Soc. **349,** 649–664 (2004) doi:10.1111/j.1365-2966.2004.07536.x

Properties of accretion shock waves in viscous flows around black holes

Sandip K. Chakrabarti[1,2]★ and Santabrata Das[1]

[1]*S.N. Bose National Centre for Basic Sciences, JD-Block, Sector III, Salt Lake, Kolkata 700098, India*
[2]*Centre for Space Physics, Chalantika 43, Garia Station Road, Garia, Kolkata 700084, India*

Accepted 2003 December 9. Received 2003 December 8; in original form 2003 October 14

ABSTRACT

Accretion flows having low angular momentum and low viscosity can have standing shock waves. These shocks arise because of the presence of multiple sonic points in the flow. We study the region of the parameter space in which multiple sonic points occur in viscous flows in the absence of cooling. We also separate the parameter space into regions allowing steady shocks and oscillating shocks. We quantify the nature of two critical viscosities which separate the flow topologies. The post-shock region being hotter, it emits harder X-rays and oscillating shocks cause oscillating X-ray intensities giving rise to quasi-periodic oscillations. We show that with the increase in viscosity parameter, the shock always moves closer to the black hole. This implies an enhancement of the quasi-periodic oscillation frequency as viscosity is increased.

Key words: accretion, accretion discs – black hole physics – shock waves.

1 INTRODUCTION

In the standard theory of thin accretion flows around black holes (Shakura & Sunyaev 1973, hereafter referred to as SS73) viscosity plays a major role. Viscosity transports angular momentum outwards and allows matter to sink into the potential well formed by the central compact object. In this model, the flow angular momentum is assumed to be Keplerian and this is the standard notion about how matter is accreted. However, Chakrabarti & Molteni (1995, hereafter referred to as Paper I), and Lanzafame, Molteni & Chakrabarti (1998, hereafter referred to as Paper II), through extensive numerical simulations showed that the angular momentum distribution depends strictly on the viscosity parameter and the way the viscous stress is defined. They showed that close to a black hole, the disc does not have a Keplerian distribution. This is because the flow must be supersonic on the horizon (Chakrabarti 1990a) whereas a Keplerian disc is always subsonic (SS73). In Papers I and II, it was shown that for a large region of the parameter space, shocks may form in accretion flows and when viscosity is increased beyond a critical value (Chakrabarti 1990a,b, 1996a, hereafter C96a), the shocks disappear.

Paper I also improved the concept of the viscosity parameter α (SS73): it argued that in a generalized flow with significant radial velocity ϑ, the viscous stress $w_{\phi r}$ should not be equated to $-\alpha\ P$ as in SS73, where P is the total pressure, but to $-\alpha_\Pi(P + \rho\vartheta^2)$ (actually, its vertically integrated value using a thin-disc approximation) where ρ is the density and the subscript Π is given to α to distinguish it from the Shakura–Sunyaev viscosity parameter. The latter prescription naturally goes over to the original prescription when radial velocity is unimportant as in the case of a standard Keplerian disc model (SS73); however, when the radial velocity is important as in the transonic flow solutions (Chakrabarti 1990a), the latter definition preserves the angular momentum even across axisymmetric discontinuities, such as accretion shocks. The reason is that, according to the Rankine–Hugoniot conditions (Landau & Lifshitz 1959), in a steady flow, the sum of the thermal pressure and ram pressure, i.e. $P + \rho\vartheta^2$ is continuous across discontinuities. This makes the viscous stress $w_{r\phi}$ continuous across axisymmetric discontinuities as well.

In an earlier study, Chakrabarti (1989a, hereafter C89a) considered the transonic properties of isothermal accretion flows and showed that for a large region of the parameter space spanned by the specific angular momentum and the temperature of the flow, an accretion disc can have standing shock waves. The specific angular momentum of the disc was smaller than that of a Keplerian disc everywhere. This flow comes about especially when the matter is accreted from the winds of a binary companion. Subsequently, Chakrabarti (1990b, hereafter C90b) showed that inclusion of viscosity reduces the region of the parameter space in that, at a sufficiently high viscosity, the Rankine–Hugoniot conditions which must be satisfied at a steady shock are not satisfied anywhere in the flow. The existence of standing shocks in sub-Keplerian inviscid accretion discs has been tested independently by several groups since then (Nobuta & Hanawa 1994; Yang & Kafatos 1995; Lu & Yuan 1997). Numerical simulations have also been carried out with several independent codes such as smoothed particle hydrodynamics (SPH) and

★E-mail: chakraba@bose.res.in

total variation diminishing (TVD) and distinct standing shocks were found exactly at the predicted locations (Chakrabarti & Molteni 1993; Molteni, Ryu & Chakrabarti 1996b).

In more recent years, it has become evident that the standing shocks may be very important in explaining the spectral properties of black hole candidates (Chakrabarti & Titarchuk 1995, hereafter CT95) as the post-shock region behaves as the boundary layer where accreting matter dissipates its thermal energy and generates hard X-rays by inverse Comptonization. C96a considered the unification of solutions of winds and accretion around compact objects. However, the cooling was treated in terms of a parameter and no parameter space was studied. The post-shock region is also found to be responsible for producing relativistic outflows (Chakrabarti 1999; Chattopadhyay & Chakrabarti 2002). Furthermore, numerical simulations indicated that the shocks may be oscillating at nearby regions of the parameter space in the presence of cooling effects (Molteni, Sponholz & Chakrabarti 1996a) and the shock oscillations correctly explain intricate properties of quasi-periodic oscillations (Chakrabarti & Manickam 2000). Recent observations support the presence of sub-Keplerian flows in accretion discs (Smith et al. 2001; Smith, Heindl & Swank 2002).

In view of the importance of the sub-Keplerian flows we plan to reinvestigate the work done on isothermal flow by C89a and C90b by extending them to the study of *polytropic flows* to check the properties of shock waves in viscous flows. What is more, unlike C89a and C90b, we investigate the behaviour of the solutions in the entire parameter space spanned by the specific energy, angular momentum and viscosity. Some work was done in C96a, but the parameter space was not explored. We find very important results: even when the viscosity parameter is very high, the flow continues to have three sonic points, a prime condition to have a standing or oscillating shock wave. However, the parameter space for standing shock waves is gradually reduced with the increase of viscosity. On the other hand, we discover that the shock location itself is reduced with the increase in viscosity parameter.

We wish to emphasize that the problem at hand is by no means a trivial extension of previous work. In an accretion flow, where the flow is subsonic at a large distance and is necessarily supersonic on the horizon, the flow has first to become supersonic at a sonic point and then, after the shock transition where it becomes subsonic, the flow must again pass through the inner sonic point before entering the black hole. In studying flows with constant energy (Chakrabarti 1989b, hereafter C89b) or isothermal flows (C89a), both the sonic points were known when the so-called 'eigenvalues', namely, the specific energy (for polytropic flow) or temperature (for isothermal flow) and the specific angular momentum are supplied. In the present situation, neither of these two quantities is constant in the flow since the viscosity will heat up the gas, increase the thermal energy and at the same time reduce the specific angular momentum as the flow proceeds towards the black hole. Thus, the inner sonic point, through which the flow will pass after the shock, is not known before the entire problem is actually solved. We have devised a novel way to solve the entire problem by iterating the location of the inner sonic point till the shock condition is satisfied. We have identified the topologies which are essential for shock formation. We have also identified the parameter space which will have solutions with three sonic points but need not have standing shocks. These solutions generally produce oscillating shocks as shown by Ryu, Chakrabarti & Molteni (1997). In C96a, some effects of viscous heating were studied and the cooling effect was chosen to be proportional to the heating effect for simplicity. No parameter space study was made. In the present paper, we ignore cooling completely. The exact effects of various cooling processes and their influence on the parameter space will be discussed elsewhere (Das & Chakrabarti 2004).

The plan of the present paper is the following: in the next section, we present the model equations. In Section 3, we present the sonic-point analysis. In Section 4, we study the global solution topology. In Section 5, we classify the parameter space in terms of whether a global solution has triple sonic points or not. In Section 6, we classify the region with triple sonic points further to indicate which region may allow standing shocks and which region may allow oscillating shocks in the presence of viscosity. We show in particular that matter with very low angular momentum may allow shocks even when the viscosity parameter is very high. In C96a it was shown that topologies are changed with viscosity and there exists two critical viscosity parameters at which such changes take place. In Section 7, we quantify these critical viscosity parameters. Finally, in Section 8 we discuss the relevance of shocks in the context of quasi-periodic oscillations and make concluding remarks.

2 MODEL EQUATIONS

We consider a steady, thin, viscous, axisymmetric accretion flow on to a Schwarzschild black hole. The space-time geometry around a Schwarzschild black hole is described by the pseudo-Newtonian potential introduced by Paczynski & Wiita (1980). Here, one uses the pseudo-Newtonian potential given by

$$g(r) = -\frac{GM}{r - 2GM_{\rm BH}/c^2}.$$

We consider the units of velocity, distance and time to be c, $r_g = 2GM_{BH}/c^2$ and $2GM_{\rm BH}/c^3$, respectively, where c is the velocity of light, and G and $M_{\rm BH}$ are the gravitational constant and the mass of the black hole, respectively. In these units, defining $x = r/r_g$, we get the potential as $g(x) = -[2(x-1)]^{-1}$. We assume the disc to be in *hydrostatic* equilibrium in the vertical direction.

In the steady state, the dimensionless hydrodynamic equations that govern the infalling matter are the following (C96a):

(i) radial momentum equation,

$$\vartheta \frac{{\rm d}\vartheta}{{\rm d}x} + \frac{1}{\rho}\frac{{\rm d}P}{{\rm d}x} - \frac{\lambda(x)^2}{x^3} + \frac{1}{2(x-1)^2} = 0; \tag{1a}$$

(ii) baryon number conservation equation,

$$\dot{M} = \Sigma \vartheta x, \tag{1b}$$

apart from a geometric constant;

(iii) angular momentum conservation equation,

$$\vartheta \frac{\mathrm{d}\lambda(x)}{\mathrm{d}x} + \frac{1}{\Sigma x}\frac{\mathrm{d}}{\mathrm{d}x}\left(x^2 W_{x\phi}\right) = 0; \tag{1c}$$

and finally

(iv) entropy generation equation,

$$\Sigma \vartheta T \frac{\mathrm{d}s}{\mathrm{d}x} = Q^+ - Q^-. \tag{1d}$$

The local variables ϑ, ρ, P and $\lambda(x)$ in the above equations are the radial velocity, density, isotropic pressure and specific angular momentum of the flow, respectively. Here Σ and $W_{x\phi}$ are the vertically integrated density (Matsumoto et al. 1984) and the viscous stress, s is the entropy density of the flow, and T is the local temperature. Q^+ and Q^- are the heat gained and lost by the flow (integrated in the vertical direction), respectively.

In our model of the disc which is assumed to be in hydrostatic equilibrium in the vertical direction, the local disc height is obtained by equating the pressure gradient force in the vertical direction with the component of the gravitational force in that direction. The half-thickness of the disc is obtained as:

$$h = a x^{1/2}(x - 1). \tag{2}$$

Here, a is the adiabatic sound speed defined as $a = \sqrt{\gamma P/\rho}$. As discussed in the introduction, we shall use the viscosity prescription of Paper I valid rigorously for flows with significant radial motion. Thus the viscous stress is:

$$W_{x\phi} = -\alpha_\Pi \Pi, \tag{3}$$

where $\Pi = W + \Sigma \vartheta^2$. As mentioned before, this will ensure that the viscous stress is continuous across the axisymmetric shock wave that we are studying here. It is to be noted that in the SS73 prescription, $W_{x\phi}$ is not continuous across the shock. Thus, the stress would transport angular momentum at different rates on two sides of the shock which would always move the shock one way or the other. This is unphysical, since in the absence of viscosity, a standing, axisymmetric shock is perfectly stable. It is impossible that an infinitesimal viscosity should destabilize the shock. However, this would have been the case if the SS73 prescription were rigorously correct.

3 SONIC-POINT ANALYSIS

At the outer edge of the accretion disc, matter has almost zero radial velocity even though it enters the black hole with the velocity of light c. Thus, during accretion, at some point, the velocity of matter should exactly match the sound speed. This point is called a critical point or a sonic point. When matter crosses a sonic point, it becomes transonic. As Chakrabarti (C89ab, C90ab) pointed out, depending on the initial parameters, a flow may have multiple sonic points and therefore, depending on whether the shock conditions are satisfied or not, a flow may or may not have a standing shock.

For the sake of completeness, we carry out the sonic-point analysis by solving the above equations (1)–(3) using a method similar to that used in C89b.

3.1 Sonic-point conditions

In the present analysis, we use the MISStress prescription (C96a) for computing Q^+, and $W_{x\phi}$ is obtained from equation (3). For the accretion flow, the entropy equation (equation 4) can be simplified as

$$\frac{\vartheta}{\gamma - 1}\left[\frac{1}{\rho}\frac{\mathrm{d}P}{\mathrm{d}x} - \frac{\gamma P}{\rho^2}\frac{\mathrm{d}\rho}{\mathrm{d}x}\right] = \frac{Q^- - Q^+}{\rho h} = C - H, \tag{4}$$

and then $H(= Q^+/\rho h)$ takes the form

$$H = Ax(ga^2 + \gamma \vartheta^2)\frac{\mathrm{d}\Omega}{\mathrm{d}x}, \tag{5}$$

where γ is the adiabatic index, $A = -\alpha_\Pi I_n/\gamma$ and $g = I_{n+1}/I_n$. Here, $\Omega(x)$ is the angular velocity of the accreting matter at the radial distance x, n is the polytropic index ($n = (\gamma - 1)^{-1}$), and I_n and I_{n+1} come from the definition of the vertically averaged density and pressure (Matsumoto et al. 1984).

In the present analysis, we use $Q_- = 0$, i.e. the cooling is ignored. This would be strictly valid if the accretion rate is low, so that the loss of energy by bremsstrahlung cooling is insignificant compared to the rest-mass energy.

After some simple algebra and eliminating $\mathrm{d}a/\mathrm{d}r$, etc. we get from the governing equations 1(a-c) and equation (2) the following first-order linear differential equation:

$$\frac{\mathrm{d}\vartheta}{\mathrm{d}x} = \frac{N}{D}, \tag{6}$$

where the numerator N is

$$N = -\frac{\alpha_\Pi A(a^2 g + \gamma\vartheta^2)^2}{\gamma x} - \left[\frac{\lambda^2}{x^3} - \frac{1}{2(x-1)^2}\right]\left[2\alpha_\Pi g A(a^2 g + \gamma\vartheta^2) + \frac{(\gamma+1)\vartheta^2}{(\gamma-1)}\right]$$
$$- \frac{\vartheta^2 a^2(5x-3)}{x(\gamma-1)(x-1)} - \frac{\alpha_\Pi g A a^2(5x-3)(a^2 g + \gamma\vartheta^2)}{\gamma x(x-1)} + \frac{2\lambda A\vartheta(a^2 g + \gamma\vartheta^2)}{x^2} \tag{7}$$

and the denominator D is

$$D = \frac{2a^2\vartheta}{(\gamma-1)} - \frac{(\gamma+1)\vartheta^3}{(\gamma-1)} - A\alpha_\Pi\vartheta(a^2 g + \gamma\vartheta^2)\left[(2g-1) - \frac{a^2 g}{\gamma\vartheta^2}\right]. \tag{8}$$

Both N and D are algebraic equations which makes this model easily tractable.

At the sonic point, both the numerator and the denominator must vanish simultaneously. For $D = 0$, one can get the expression for the Mach number, $M(x_c)$, at the sonic point and it is given by

$$M(x_c) = \sqrt{\frac{-m_b - \sqrt{m_b^2 - 4m_a m_c}}{2m_a}} \tag{9}$$

where

$$m_a = -A\alpha_\Pi\gamma^2(\gamma-1)(2g-1) - \gamma(\gamma+1),$$

$$m_b = 2\gamma - 2A\alpha_\pi g\gamma(\gamma-1)(g-1)$$

$$m_c = A\alpha_\Pi g^2(\gamma-1).$$

In the weak viscosity limit, $\alpha_\Pi \to 0$ and the Mach number at the sonic point is

$$M(x_c) \approx \sqrt{\frac{2}{\gamma+1}}$$

for $\alpha_\Pi \to 0$, a result obtained in C89b.

Setting $N = 0$, we get an algebraic equation for the sound speed at the sonic point, which is given by

$$F(\mathcal{E}_c, \lambda_c, x_c) = -\left[\frac{\alpha_\Pi A\{g+\gamma M^2\}^2}{\gamma x} + \frac{\alpha_\Pi A(5x-3)\{g+\gamma M^2\}}{\gamma x(x-1)} + \frac{M^2(5x-3)}{x(\gamma-1)(x-1)}\right]a^2$$
$$+ \frac{2\lambda A M(g+\gamma M^2)}{x^2}a - \left[\frac{\lambda^2}{x^3} - \frac{1}{2(x-1)^2}\right]\left[2\alpha_\Pi g A(g+\gamma M^2) + \frac{(\gamma+1)M^2}{(\gamma-1)}\right] = 0. \tag{10}$$

We solve the above quadratic equation to obtain the sound speed at the sonic point. Das et al. (2001) suggested that, depending on a given set of initial parameters, the accretion flow may have a maximum of four sonic points where one of the sonic points always lies inside the black hole horizon for non-dissipative accretion flow. In our present study, we also expect a similar result.

3.2 Nature of the sonic points

A black hole accretion is always transonic. Thus the originally subsonic matter definitely has to pass through the sonic point to become supersonic before entering the black hole. Depending on the initial parameters, a flow may have multiple sonic points. The nature of the sonic point depends on the value of the velocity gradients at the sonic point. It is easy to show that $\mathrm{d}\vartheta/\mathrm{d}x$ assumes two values at the sonic point. One of them is valid for the accretion flow and the other is valid for the wind. If both the derivatives are real and of opposite signs, the sonic point is saddle type. When the derivatives are real and of the same sign, the sonic point is nodal type. When the derivative is complex, the sonic point is spiral type (or O-type, for non-dissipative flow). See C90b for details of the classifications. In order to form a standing shock, the flow must have more than one saddle-type sonic point.

In Fig. 1(a) we plot the variation of specific angular momentum (λ_c) as a function of the logarithmic sonic-point location (x_c) for a given viscosity parameter ($\alpha_\Pi = 0.1$). Here different curves are drawn for different specific energies at the sonic points. The energies, from the top curve to the bottom, are given by: $\mathcal{E}_c = 0.0007,\ 0.001,\ 0.003,\ 0.005,\ 0.007,\ 0.011,\ 0.015,\ 0.019,\ 0.023$ and 0.027, respectively. The long-dashed curve at the top represents the Keplerian angular momentum distribution which is completely independent of the initial flow parameters and depends only on the geometry. The solid part of the curves represents the saddle-type sonic points, the dotted part of the curves represents the nodal-type sonic points and the short-dashed part of the curves are for the spiral-type sonic points. First notice that the sonic points always occur at angular momentum below the Keplerian value. Notice that for lower values of the specific energy at the sonic point, an accretion flow contains all three types of sonic points in a systematic order: saddle–nodal–spiral–nodal–saddle for a monotonic increase of the location of the sonic points. With the increase of energy $\mathcal{E}_c$ the region of spiral-type sonic points gradually decreases and is finally replaced by the nodal-type sonic points, though multiple sonic points still exist. The shaded area separates the nodal-type sonic-point region in the λ_c–x_c plane. With further increase of energy all the nodal-type sonic points also disappear and are replaced by saddle-type sonic points. In this case, the flow has only one sonic point for a given sub-Keplerian angular momentum. Thus, for a given angular momentum of the flow, there exists

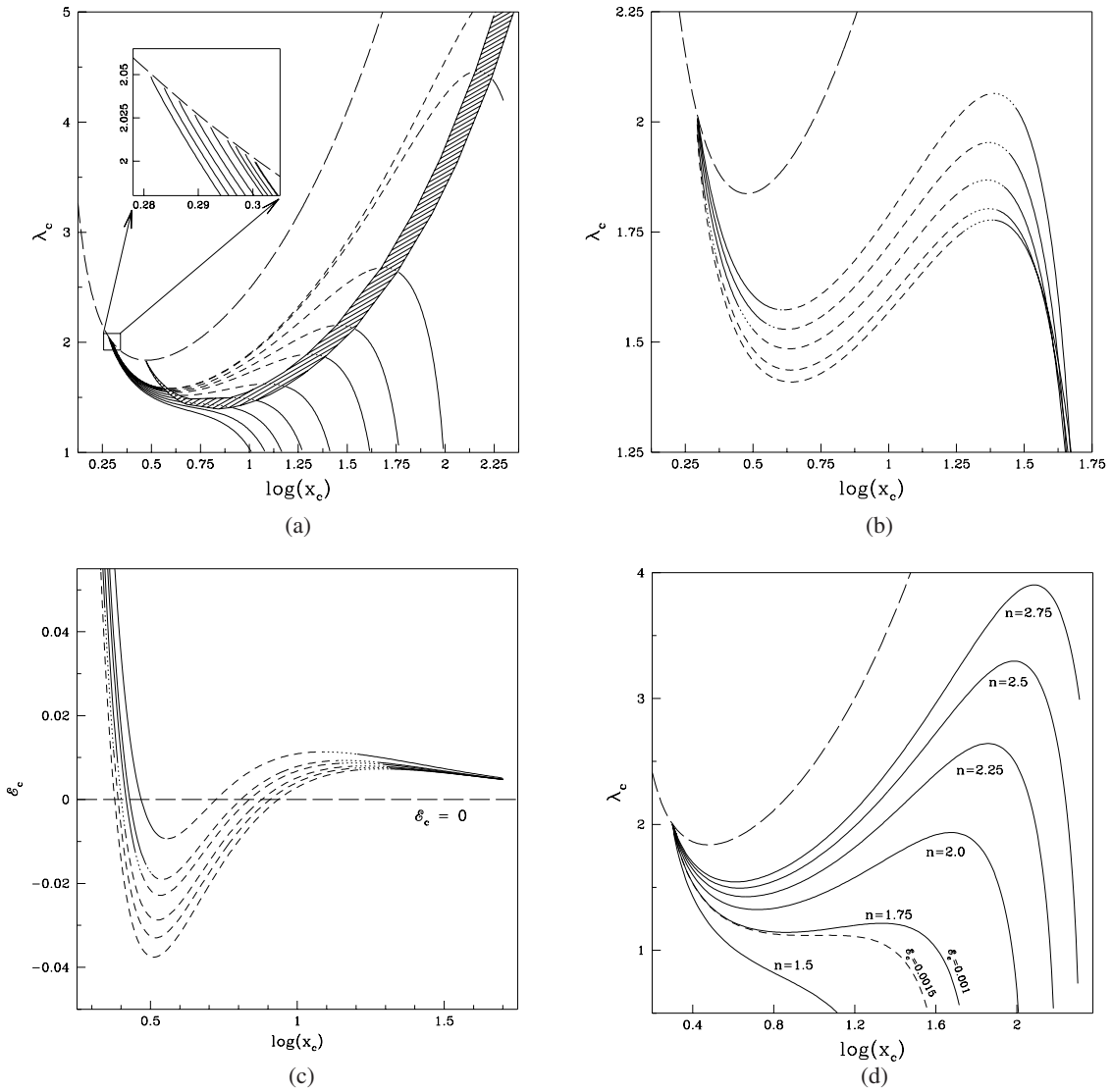

Figure 1. (a) Variation of specific angular momentum (λ_c) as a function of the logarithmic sonic-point location (x_c) for the viscosity parameter ($\alpha_\Pi = 0.1$). The long-dashed curve is the Keplerian angular-momentum distribution. The solid curves represent the saddle-type sonic points, dotted curves represent the nodal-type sonic points and the short-dashed curves are for the spiral-type sonic points. The shaded area is the nodal-type sonic-point region. (b) Variation of angular momentum at the sonic point as the viscosity parameter is varied. The specific energy at the inner sonic point is held fixed at 0.006. From the uppermost to the lowermost curve: $\alpha_\Pi = 0$, 0.2, 0.4, 0.6 and 0.7, respectively. Other notation is the same as in (a). (c) Variation of the specific energy at the inner sonic point as a function of the viscosity parameter α_Π. From the uppermost curve to the lowermost curve, $\alpha_\Pi = 0$, 0.25, 0.35, 0.5, 0.6 and 0.7, respectively. Other notation is the same as in (a). (d) Variation of the specific angular momentum at the inner sonic point as a function of the polytropic index n (marked on each curve). Generally, the number of sonic points decreases by decreasing n. The specific energy has been kept fixed at 0.001 except for the dashed curve where it is 0.0015, to show that for a given polytropic index, the number of sonic points increases with decreasing energy.

a range of energy $\mathcal{E}_{\rm min} < \mathcal{E}_c < \mathcal{E}_{\rm max}$ such that the flow has multiple sonic points. In the inset, we zoom in on a small portion of the curve close the Keplerian value to highlight the fact that the angular momentum at the sonic point always remains sub-Keplerian when the cooling process is ignored. In the future (Das & Chakrabarti, 2004), we shall show that a flow can also be super-Keplerian when cooling is added.

In Fig. 1(b) we show a very important aspect of viscous transonic flow. Here we show how the angular momentum at the sonic point varies when the viscosity parameter α_Π is increased. We hold the energy at the sonic point fixed at $\mathcal{E}_c = 0.006$. In the absence of viscosity ($\alpha_\Pi = 0$, the uppermost curve), the flow has all three types of sonic points. Similar to Fig. 1(a), here we also indicate the saddle-, nodal- and spiral-type sonic points by the solid, dotted and short-dashed curves, respectively. The uppermost long-dashed curve represents the Keplerian angular momentum distribution. With the increase of α_Π, more and more inner saddle-type sonic points are replaced by nodal-type sonic points and similarly nodal-type sonic points are also replaced by spiral-type sonic points. The curves, from the uppermost to the lowermost, are for $\alpha_\Pi = 0$, 0.2, 0.4, 0.6, 0.7, respectively. For $\alpha_\Pi = 0.7$, all the inner saddle-type sonic points disappear and only the spiral-type points remain. Thus there exists a critical viscosity parameter $\alpha_{\Pi(c,i)}$ at a given $\mathcal{E}_{\rm in}$ for which all the inner saddle-type sonic points are completely converted into spiral-type points. In this case, the flow has no choice but to pass through the outer sonic point only. The existence of such

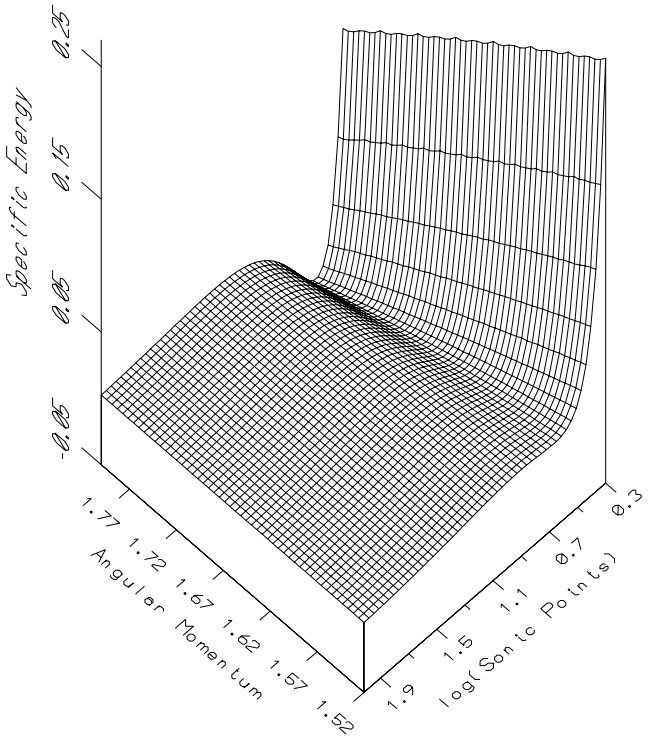

Figure 2. A gradual change in the number of physical sonic points is easily seen in this three-dimensional view of $F(E_c, \lambda_c, x_c) = 0$ (equation 9) surface. At high angular momenta there are three sonic points, but they merge to become one at lower angular momenta. $\alpha_\Pi = 0.01$ has been chosen.

critical viscosities has been predicted in C90ab and C96a – below we compute their values exactly as a function of the inflow parameters. This behaviour also hints at the conclusion that the parameter space for the existence of a transonic flow may shrink with increase of viscosity.

We continue our investigation of the transonic nature of the flow and have replotted in Fig. 1(c) a figure similar to Fig. 1(a) but we increase α_Π gradually while keeping the specific angular momentum at the sonic point fixed ($\lambda_c = 1.65$). Values of α_Π are, from the top to the bottom curve, $\alpha_\Pi = 0$, 0.25, 0.35, 0.5, 0.6 and 0.7, respectively. Solid, dotted and short-dashed lines represent the saddle-type, nodal-type and spiral-type sonic points, respectively. The long-dashed line separates the positive and negative energy regions in the $\mathcal{E}_c$–x_c plane. Notice that, for increasing α_Π, saddle-type sonic points are gradually replaced by the nodal- and spiral-type sonic points: outer saddle-type sonic points recede further away and the inner saddle sonic points proceed toward the black hole horizon. For $\alpha_\Pi = 0.7$, the inner saddle-type sonic points completely disappear and become spiral type. This behaviour points to a critical value of the viscosity parameter ($\alpha_{\Pi,c}$) which separates the accretion flow from the multiple sonic-point regime to the single sonic-point regime at a given λ_c. It is also clear that at the same sonic point, the specific energy steadily decreases for increasing α_Π. This is because, when α_Π is increased, the accreting matter tends to become a Keplerian disc closer to the black hole and becomes more strongly bound with lower energy. Note that the energy at the outer sonic point always remains positive for all initial parameters.

In our final study of the nature of the sonic points, we chose n, the polytropic index, to be our free parameter. For a highly relativistic flow, or a radiation-dominated flow, $n = 3$, but for a monatomic, non-relativistic gas, $n = 3/2$. In Fig. 1(d) we show the variation of λ_c with sonic-point location x_c. We keep the specific energy at the sonic point to be 0.001. The long-dashed curve is the Keplerian distribution as before. We note that with the increase of the adiabatic index γ, i.e. decrease of the polytropic index n, the number of sonic points decreases from three to one. In this example, in the extreme non-relativistic regime ($n = 1.5$) the accretion flow has a single saddle-type sonic point for any specific angular momentum. For the same energy, for $n = 1.75$ there are three sonic points, indicating that a standing or an oscillating shock in the flow may be possible. In this figure, we also show that for a given n (such as for $n = 1.75$) if we increase the energy at the sonic point ($\mathcal{E}_c = 0.0015$), multiple sonic points disappear and a single sonic point forms. This indicates that there must be a critical value of $\mathcal{E}_c = \mathcal{E}_{\rm cri}$ associated with each n above which multiple sonic points do not exist when all other parameters are kept fixed.

The general behaviour of the flow at the sonic point is best seen in Fig. 2, where we depict the surface $F(\mathcal{E}_c, \lambda_c, x_c) = 0$ (equation 9) for $\alpha_\Pi = 0.01$. Sonic points x_c are plotted along the X-axis in the logarithmic scale, λ_c is plotted along the Y-axis and $\mathcal{E}_c$ is plotted along the Z-axis. At high angular momenta, there are three sonic points, but they merge to become one at lower angular momenta. Below a critical value $\lambda_{\rm cri}$, the flow does not have more than one sonic point.

4 GLOBAL SOLUTION TOPOLOGY

A basic criterion for studying shock properties is that the accretion flow must have multiple saddle-type sonic points and the shock should join two solutions – one passing through the outer sonic point and the other passing through the inner sonic point. The solution topologies

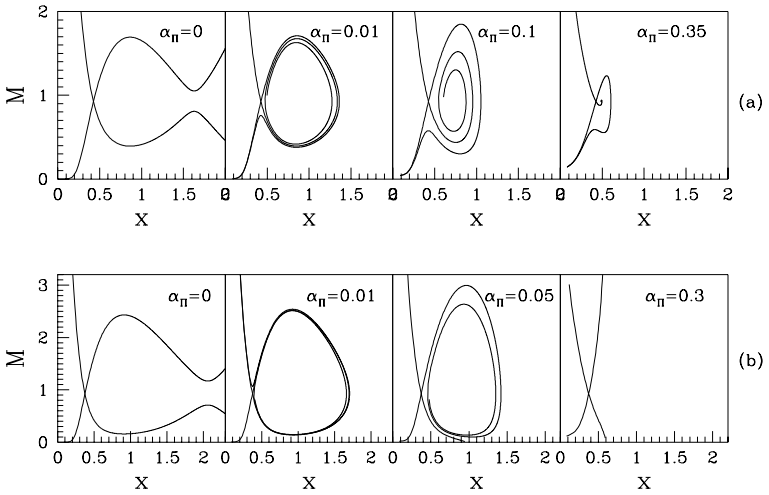

Figure 3. Variation of global solution topologies of the viscous accretion flow around black holes. In (a), drawn for $\lambda(x_{\rm in} = 2.665) = 1.68$, the four panels show how the open topology at lower viscosity becomes closed at higher viscosity. In (b), drawn for $\lambda(x_{\rm in} = 2.359) = 1.78$, the closed topology opens up again.

have already been discussed in C96a. The current paper studies in greater detail the topologies associated with $f = 1$ of C96a. In particular, we show below new pathways through which topologies may vary.

In Figs 3(a)–(b) we have shown how the flow topologies change with the viscosity parameter α_Π and the specific angular momentum $\lambda_{\rm in}$ at the inner sonic point $x_{\rm in}$. Two distinct types of behaviour have been highlighted here: one at a low angular-momentum regime (Fig. 3a) and the other at a high angular-momentum regime (Fig. 3b). In Fig. 3(a) we keep the inner sonic point fixed at $x_{\rm in} = 2.665$ and the specific angular momentum at this point is $\lambda_{\rm in} = 1.68$. At low angular momentum and without viscosity (the box at the extreme left in Fig. 3a) the subsonic flow enters the black hole after passing through the inner sonic point. In the second box, the viscosity is slightly higher and topologies are closed for the same inner sonic point. So, for a given set of parameters, there must be a critical viscosity parameter ($\alpha_{\Pi c}$) for which open topologies become closed topologies. We will discuss critical viscosity rigorously in Section 7. Accretion with parameters causing this kind of topology never joins with any Keplerian disc unless a shock is formed (this will be shown below). When a standing shock formation is not possible, an accretion flow passes through the outer sonic point directly before falling into the black hole. For a further increase of α_Π (next two boxes) the closed topology shrinks gradually and finally disappears leaving behind only the outer sonic point (Bondi type). This is directly analogous to the shrinking of the phase space of a simple harmonic oscillator in the presence of damping (C90a). These solutions are basically the same as the $f = 1$ case of fig. 2(a) of C96a.

In Fig. 3(b), where solutions are plotted with a higher specific angular momentum at the inner sonic point ($x_{\rm in} = 2.359$ and $\lambda_{\rm in} = 1.78$), the explanations of the first and second boxes is similar to the earlier ones (Fig. 3a), but in the third box ($\alpha_\Pi = 0.05$) the accretion flow topology reverses its direction of spiraling and the flow can join with a Keplerian disc very close to a black hole. All the differences between these two figures (Figs 3a and b) are mainly due to the difference of specific angular momentum at the sonic point rather than the change of sonic-point locations. In Fig. 11 (below), we will show that the nature of the accretion flow topologies have a strong dependence on the angular momentum at the sonic point. For a higher α_Π (next two boxes) the Keplerian disc comes even closer to the black hole and topologies passing through the inner sonic point becomes Bondi type. We suspect that two limits of viscosity parameters would cause an oscillation of the inner part of the Keplerian disc, but we cannot be certain about it without a time-dependent numerical simulation.

In order to show that flow topologies often can take new pathways than what was already known (C96a), in Fig. 4 we have plotted solution topologies passing through the outer sonic point chosen at $x_{\rm out} = 25r_g$ and the specific angular momentum $\lambda(x_{\rm out})$ is 1.8. The viscosity parameter is varied (marked on each box). For a lower α_Π, the topologies are closed as in fig. 4 of C96a and a flow having this topology cannot be transonic anyway. When α_Π is increased, closed topologies gradually open up (unlike C96a where $x_{\rm out} = 35$ was chosen and the opening of the topologies did not occur) and if the shock condition is satisfied, the accretion flow passing through the outer sonic point jumps into the subsonic branch and goes through the inner sonic point before entering the black hole. For higher α_Π, the same outer sonic point no longer remains saddle type. First it becomes nodal type and then it becomes spiral type (Fig. 1a). Considering that the outer sonic point recedes farther away with the increase of α_Π, this behaviour is not surprising. This, together with fig. 4 of C96a, shows that there could be more than one way of reaching a nodal topology.

5 CLASSIFICATION OF THE PARAMETER SPACE

An important part of understanding a viscous flow is to classify the parameter space as a function of the viscosity parameter. In Fig. 5 we have separated the parameter space for the accretion flow which can pass through the inner sonic point. The angular momentum at this sonic point ($\lambda_{\rm in}$) is varied along the X-axis and the corresponding specific energy at the inner sonic point ($\mathcal{E}_{\rm in}$) is plotted along the Y-axis. The

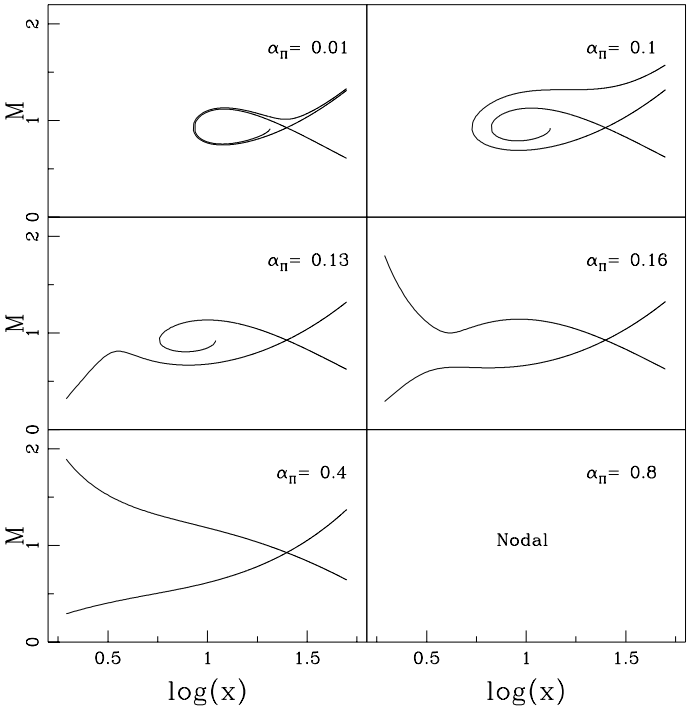

Figure 4. Variation of global solution topologies of the viscous accretion flows when the outer sonic point is kept fixed at $x_{\rm out} = 30r_g$ while the viscosity parameter is varied. The closed topologies (with one saddle type and a spiral type at the centre) at lower α_Π become open. Eventually, the saddle type also disappears to produce a nodal-type sonic point.

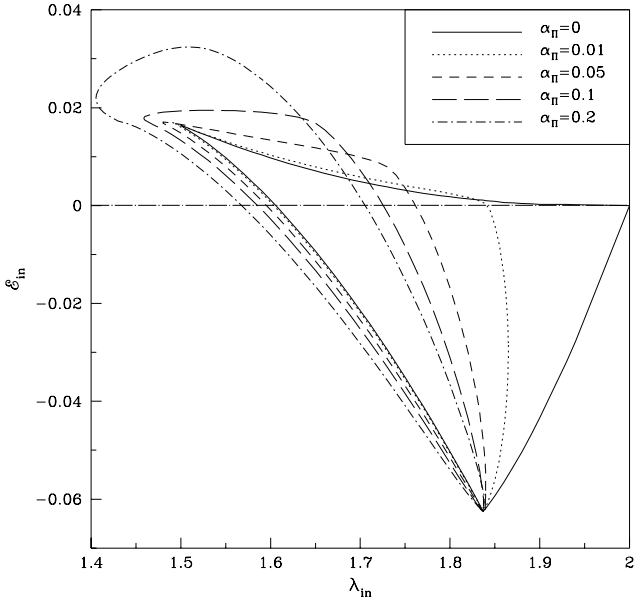

Figure 5. Classification of the parameter space spanned by the specific energy and the specific angular momentum of the flow at the inner sonic point. The bounded regions drawn for different viscosity parameters (marked in the inset) contain allowed solutions which may pass through the inner sonic point. As the viscosity increases, the region shifts towards lower angular momentum and higher energy.

region bounded by a given curve contains a parameter space in which multiple sonic points are possible. For instance, for $\alpha_\Pi = 0$, the region bounded by the solid curve is identical to the region found by C89b. For increasing α_Π, the region of multiple saddle-type sonic points is reduced near the high angular-momentum side, while it increases in the lower angular-momentum side. It may be recalled (C89b and Fig. 1a) that at low angular momentum, the number of sonic points is just one. With the rise of α_Π, the angular momentum at the sonic point is increased, increasing the number of sonic points. At a higher angular momentum, the situation is just the opposite. In this case, there are already multiple sonic points for $\alpha_\Pi \sim 0$ and for high enough α_Π, viscosity transports angular momentum very rapidly causing a steep rise in angular momentum itself. This, in turn, means that the flow can have only one saddle-type sonic point in this case.

6 STANDING SHOCKS AND FURTHER CLASSIFICATION OF THE PARAMETER SPACE

Although, in general astrophysical contexts, shocks are ubiquitous and possibly non-stationary, in an accretion flow, the location, strength and thermodynamic quantities may be quantified very exactly by using the Rankine–Hugoniot conditions (RHCs). The study is similar to the study of shocks in solar winds (e.g. Holzer & Axford 1970) and white-dwarf surfaces.

The shock conditions which we employ here are the usual RHCs presented in C89b, i.e. (a) the local energy flux is continuous across the shock; (b) the mass flux is continuous across the shock; (c) the momentum balance condition is satisfied; and finally (d) angular momentum should be continuous across the axisymmetric shock.

The way an accretion flow moves around a black hole, as seen from the local rotating frame, is as follows. First the flow, subsonic at a very large distance, passes through the outer sonic point and becomes supersonic. The RHCs then decide whether a shock will be formed or not. Of course, our consideration of satisfying the RHCs at a given location holds only if the shock is thin, i.e. viscosity is low. Nevertheless, we continue to use this prescription at higher viscosities to have a first-order guess of the shock location. Similarly, we assume that there is no excess source of torque at the shock itself, so that the angular momentum may be assumed to be continuous across it. This condition may be violated when magnetic fields are present. In the presence of large-scale poloidal magnetic fields, there could be magnetic torques which could make the flow angular momentum discontinuous.

6.1 Method of calculating the shock locations

Accretion flow first passes through the outer sonic point and becomes supersonic. It then jumps to the subsonic branch through a shock. This subsequently passes through the inner sonic point before disappearing into the black hole. In our present study we begin a numerical integration from the inner sonic point and proceed towards the outer edge of the accretion disc to look for the shock location. During integration along the subsonic branch, it is possible to calculate all the local variables (i.e. ϑ, a, M, ρ) at the post-shock region, in terms of the initial flow parameters. We calculate the total pressure, local flow energy, and specific angular momentum at the shock using these subsonic local variables. At the shock, the total pressure, local flow energy, mass accretion rate (one of the flow parameters) and specific angular momentum are conserved. These conserved quantities at the shock give the other set of supersonic local variables for the supersonic branch. This supersonic set of local variables helps us to find the outer sonic point uniquely for an accretion flow with fixed inner sonic point and other initial flow parameters when integration takes place towards the outer edge of the black hole. Thus, the accretion flow can be connected with both saddle-type sonic points through the shock for a dissipative system and this determines the standing shock location for a given set of initial parameters.

We compute the supersonic local flow variables in terms of the subsonic local flow variables in the following way.

Our model accretion flow is in vertical equilibrium and the total pressure of the accretion flow at any given point is given by

$$\Pi = W + \Sigma\vartheta^2, \tag{11}$$

where W and Σ are the vertically averaged thermal pressure and density, respectively.

We use the mass conservation equation (equation 1b) in equation (10) and calculate the sound speed a in terms of the radial velocity (ϑ) at the shock, x_s, in the supersonic branch, which is given by

$$a^2 = \mathcal{C}_1\mathcal{C}_2\vartheta - \mathcal{C}_2\vartheta^2, \tag{12}$$

where

$$\mathcal{C}_1 = \frac{4\pi\Pi x_s}{\dot{M}I_n}$$

and $\mathcal{C}_2 = \gamma/g$.

From the local flow energy equation, the radial velocity ϑ at the shock in the supersonic branch can be calculated using equation (11) and is given by

$$\vartheta = \frac{-\vartheta_b + \sqrt{\vartheta_b^2 - 4\vartheta_a\vartheta_c}}{2\vartheta_a}, \tag{13}$$

where $\vartheta_a = 2n\mathcal{C}_1\mathcal{C}_2$, $\vartheta_b = -2n\mathcal{C}_1\mathcal{C}_2$,

$$\vartheta_c = 2\mathcal{E} - \frac{\lambda^2(x_s)}{x_s^2} + \frac{1}{(x_s - 1)}$$

and $\mathcal{E}$ is the local flow energy.

Here, the total pressure and flow energy at the shock are calculated with the help of the subsonic flow variables. We consider only the '+' sign as we are interested in finding the local flow variables in the supersonic branch. This radial velocity is used to get the sound speed (equation 12) in the supersonic branch of the flow. This is used to obtain the outer sonic point by using numerical integration. We thus have a complete solution with a standing shock in a viscous flow.

In Fig. 6(a) we have shown how a shock may be formed by joining two solutions, one with a lower entropy passing through the outer sonic point, and the other with a higher entropy passing through the inner sonic point. Two curves are drawn for two different energies (marked). $\mathcal{E}_{\rm in}$ and $\mathcal{E}_{\rm out}$ are the energies at the inner and outer sonic points for a shocked accretion flow which has a standing shock. Due to viscous heating processes, energy is increased and the shock wave is formed when the flow jumps from the lower-energy solution to the higher-energy solution. If we included only the cooling process, the situation would have been reversed. The flow parameters are $x_{\rm out} = 39.7$, $\lambda_{\rm in} = 1.65$,

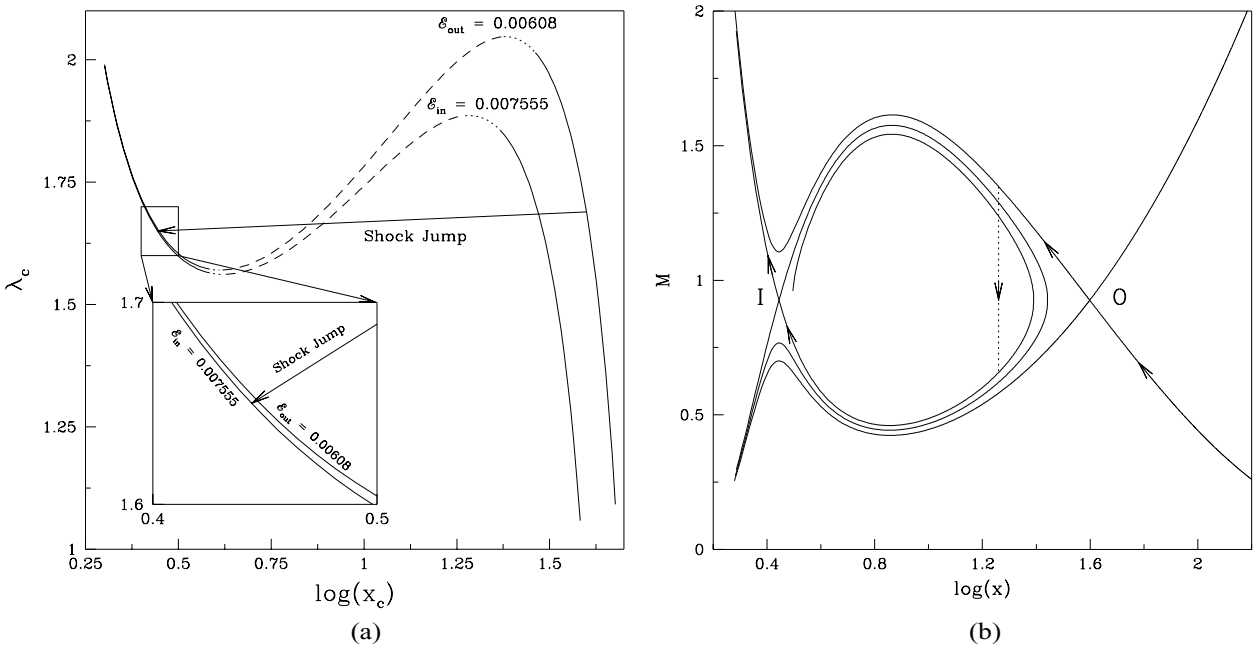

Figure 6. (a) An example of how a standing shock might form in viscous transonic flows is depicted here. Flow passing through the outer sonic point at $x_{\rm out} = 39.7$ and energy $\mathcal{E}_{\rm out} = 0.00608$ has a shock and passes through the inner sonic point at $x_{\rm in} = 2.78$ where its energy is $\mathcal{E}_{\rm in} = 0.007555$. The inset shows the details. (b) The actual solution topology for the case discussed in (a) is shown here which, along with the outer (O) and inner (I) sonic points, also shows the shock transition at $x_s = 18.2$ (vertical dotted line). The arrowed curve is followed by a flow while entering the black hole.

$\alpha_\Pi = 0.05$ and $\gamma = 4/3$. The shock condition uniquely determines the inner sonic point, which is at $x_{\rm in} = 2.78$. The end positions of the long arrow mark the locations of the sonic points. In the inset, we zoom in on a selected region in the λ_c–x_c plane to show explicitly that the angular momentum is indeed decreased.

In Fig. 6(b) we present the complete solution of the flow which includes a standing shock in a viscous flow for the same set of parameters used to draw Fig. 6(a). The arrows indicate the direction of the accreting flow. Subsonic accreting flow passes through the outer sonic point (O) and becomes supersonic. At x_s, the shock conditions are satisfied – the flow jumps from the supersonic branch to the subsonic branch and subsequently passes through the inner sonic point (I). In this particular case, the shock conditions are satisfied at $x_s = 18.2$ and the shock is denoted by the dotted vertical line.

6.2 Parameter space which allows standing shocks

In Fig. 5 we have already classified the parameter space in terms of the number of sonic points in the flow. Here, in Fig. 7, we concentrate on the region which allows only standing shocks in a viscous flow. The viscosity parameters are marked. The region marked $\alpha_\Pi = 0$ coincides with that in C89b and in Chakrabarti (1996b, 1998, hereafter C96b and C98, respectively) when appropriate models are considered. Compared to the inviscid case, the effective region of the parameter space shrinks in the high angular-momentum side when the viscosity is increased. The situation is exactly the opposite at the lower angular-momentum side. We observe that even at angular momentum as low as 1.4, standing shocks could be formed if the viscosity is high enough. Above a critical viscosity (which depends on other parameters as will be shown in Fig. 13 below), this region disappears completely.

We continue our study of the parameter space which may allow multiple sonic points. In Fig. 8 we show a curious feature: the mapping between the post-shock parameters and the pre-shock parameters. We plot the region of the post-shock parameters at the inner sonic point ($\mathcal{E}_{\rm in}$, $\lambda_{\rm in}$) (bounded by the solid curve) and the region of the pre-shock parameters at the outer sonic point ($\mathcal{E}_{\rm out}$, $\lambda_{\rm out}$) (bounded by the long-dashed curve) for a shock which is determined through the RHCs for $\alpha_\Pi = 0.01$. For each and every point in the pre-shock parameter space region, there exists a point in the post-shock parameter space region and therefore we have a complete solution. For definiteness, we also show vertical dashed and dotted lines in the two different angular-momentum ranges in the post-shock parameter space region in which $\lambda_{\rm in}$ is kept fixed but $\mathcal{E}_{\rm in}$ is varied. The corresponding pre-shock parameters form a curve, indicating that both the angular momentum and the energy had to be adjusted to get the self-consistent solution. In a non-dissipative flow, there is no variation of energy and angular momentum in the accretion flow. As a result, both the inner and outer sonic-point parameter spaces merge (C89b; C98).

6.3 Parameter space which may allow oscillating shocks

An important role that is played by oscillating shocks is to produce the so-called quasi-periodic variations of the X-ray intensity from galactic black hole candidates. In inviscid flow, the region of the parameter space which produced multiple sonic points, but where the RHCs were

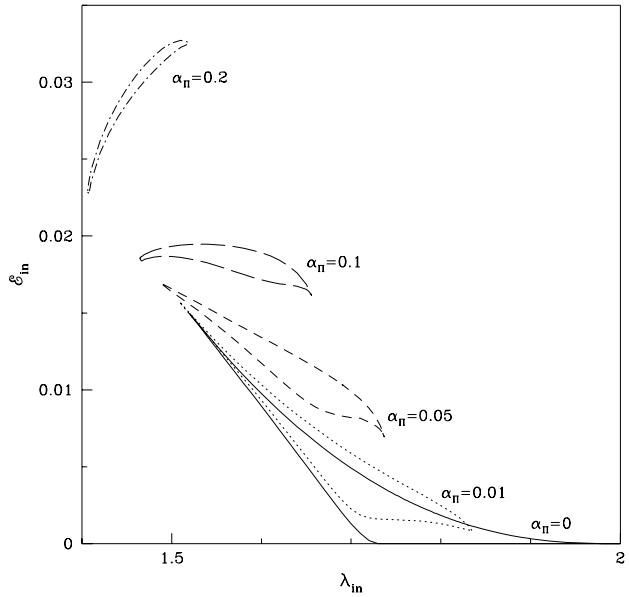

Figure 7. Variation of the region of the parameter space which forms a standing shock as a function of the viscosity parameter α_Π. The region shrinks with the increase of viscosity parameter.

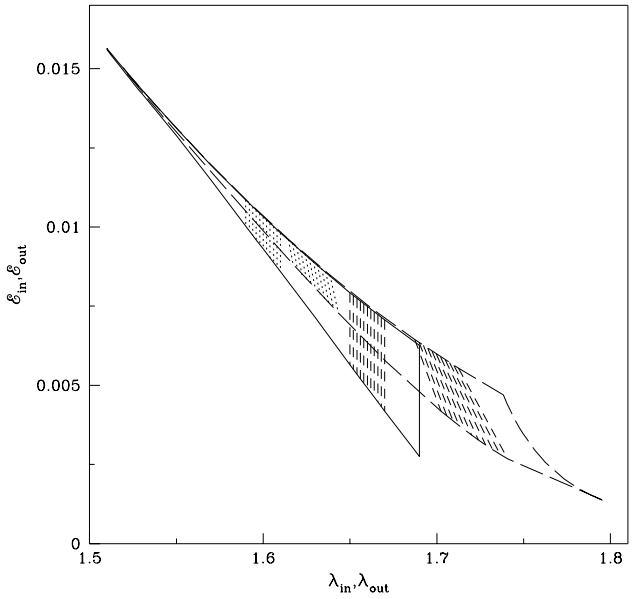

Figure 8. Mapping of the parameter space of the pre-shock region (solid boundary) spanned by ($\mathcal{E}_{\rm in}$, $\lambda_{\rm in}$) onto the parameter space in the post-shock region (dashed boundary) spanned by ($\mathcal{E}_{\rm out}$, $\lambda_{\rm out}$) in a viscous flow ($\alpha_\Pi = 0.01$).

not satisfied, was important for this type of oscillating shocks (Ryu et al. 1997). Here, winds are also produced sporadic from the post-shock region. In the presence of cooling, especially when the cooling time-scale roughly agrees with the infall time-scale, a new phenomenon occurs. Here, a steady shock may exhibit oscillations when time-dependent simulation is carried out.

It is to be noted that it is, in a general flow, very difficult to divide the parameter space in terms of whether the shock will exist or not. This is because, when there are shocks, at least the RHCs allow us to map the pre-shock and the post-shock flow parameters (see Fig. 8). When there are no shocks, however, it is not straightforward to map these two sets of parameters. Thus, one has to rely on global topological behaviour of the flow solutions and whether they allow multiple sonic points.

One of the criteria to use is to check which parameter space allows one to have the inner sonic-point energy larger than the outer sonic-point energy. For instance, in Fig. 9(a) we plotted the inner sonic-point energy ($\mathcal{E}_{\rm in}$) along the X-axis and the outer sonic-point energy ($\mathcal{E}_{\rm out}$) along the Y-axis for a set of inner sonic-point angular momentum ($\lambda_{\rm in}$) when accretion flows pass through shocks. It is clear that $\mathcal{E}_{\rm out}$ varies almost linearly with $\mathcal{E}_{\rm in}$ and the nature of this variation depends only on $\lambda_{\rm in}$. It is not unwarranted to assume that a similar linear variation

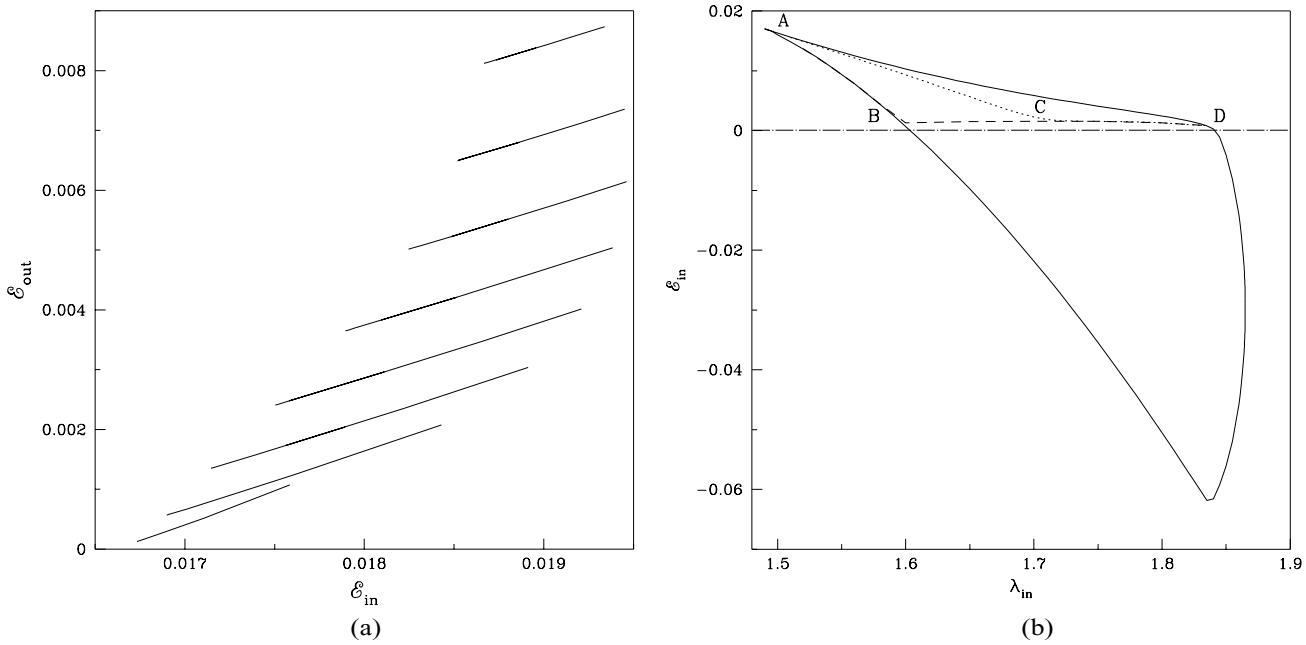

Figure 9. (a) Example of variation of the outer sonic-point energy $\mathcal{E}_{\rm out}$ as a function of the inner sonic-point energy $\mathcal{E}_{\rm in}$ when the flow has a shock. $\alpha_\Pi = 0.1$ and $\lambda(x_{\rm in}) = 1.50$ for the topmost curve. Curves have an increment of $\Delta\lambda(x_{\rm in}) = 0.02$ while going towards the bottom. (b) Division of the parameter space ($\mathcal{E}_{\rm in}$, $\lambda_{\rm in}$) for a viscosity parameter ($\alpha_\Pi = 0.01$) on the basis of the number of sonic points. The region separated by the dotted line has more than one X-type (saddle-type) sonic point and flows in this region form standing shocks. The region surrounded by the dashed curve has more than one X-type sonic point but the Rankine–Hugoniot conditions are not satisfied here.

will continue for shock-free solutions also at least if the viscosity is low. Assuming this, we extrapolate this variation in shock-free solutions towards lower values of $\mathcal{E}_{\rm in}$ till $\mathcal{E}_{\rm out} \sim 0$, keeping $\lambda_{\rm in}$ constant. In doing so, we ensured that the accretion flow topology which passes through the inner sonic point must remain closed (Figs 3a–b). We follow this procedure to estimate the cut-off $\mathcal{E}_{\rm in}$ for different $\lambda_{\rm in}$ and obtain the region in the parameter space where the accretion flow has more than one X-type sonic point.

In Fig. 9(b) we show the division of the parameter space ($\mathcal{E}_{\rm in}$, $\lambda_{\rm in}$) for the viscosity parameter $\alpha_\Pi = 0.01$ on the basis of the number of sonic points. Flows with parameters from the region ACD have more than one X-type (saddle-type) sonic point and the RHCs are also satisfied. Flows with parameters from the region ABC have more than one X-type sonic point but the RHCs are not satisfied here. From our previous experience with non-dissipating flows, we predict that those solutions with multiple sonic points which do not produce standing shocks must be producing oscillating shocks. This region becomes bigger when the viscosity parameter is reduced. The rest of the parameter space gives solutions with a closed topology passing through the inner sonic point.

6.4 Parameter space for all possible solutions

Fig. 10 shows the classification of the parameter space in the energy–angular momentum ($\mathcal{E}_{\rm in}$, $\lambda_{\rm in}$) plane in terms of different accretion flow topologies (small box) for $\alpha_\Pi = 0.01$. The solid boundary separates the region in the parameter space for closed topologies passing through the inner sonic point in general. Further subclasses are indicated by the dotted, dashed and dot-dashed curves which classified the solution topologies depending on their behaviour. Examples of solution topologies with initial parameters taken from different regions (marked) of the parameter space are plotted in seven small boxes (marked). All the small boxes depict Mach number variation as a function of the logarithmic radial distance. The box labelled S shows an accretion flow solution which passes through a shock. The dotted vertical line with an arrow indicates the location of the standing shock. The solution drawn in the box marked OS is an accretion flow which has multiple sonic points but does not satisfy the RHCs after the flow becomes supersonic. From our earlier experience with an inviscid flow, this topology is expected to give rise to an oscillating shock solution. The box marked OAC shows a new type of solution topology having multiple sonic points. One branch of the topology is closed and the other branch is open. This kind of solution is available in a small region of the parameter space shown in the inset on the upper-right corner. Solutions inside the CI1 box have closed topology (inner spiral going anticlockwise) having only one saddle-type sonic point and this kind of solution belongs to a large region of the parameter space with a relatively lower angular-momentum region. The box CI2 shows a similar result as CI1 but here the nature of the topology is different (inner spiral going clockwise) and this type of solution exists in a higher angular-momentum region. The box labelled I* represents an accretion flow solution which only passes through the inner sonic point. This solution could be for an accretion or wind and the initial parameters for this type of topology belong to the region indicated by I* in the parameter space. The topology with parameters taken from the O* region of the parameter space is also plotted in the

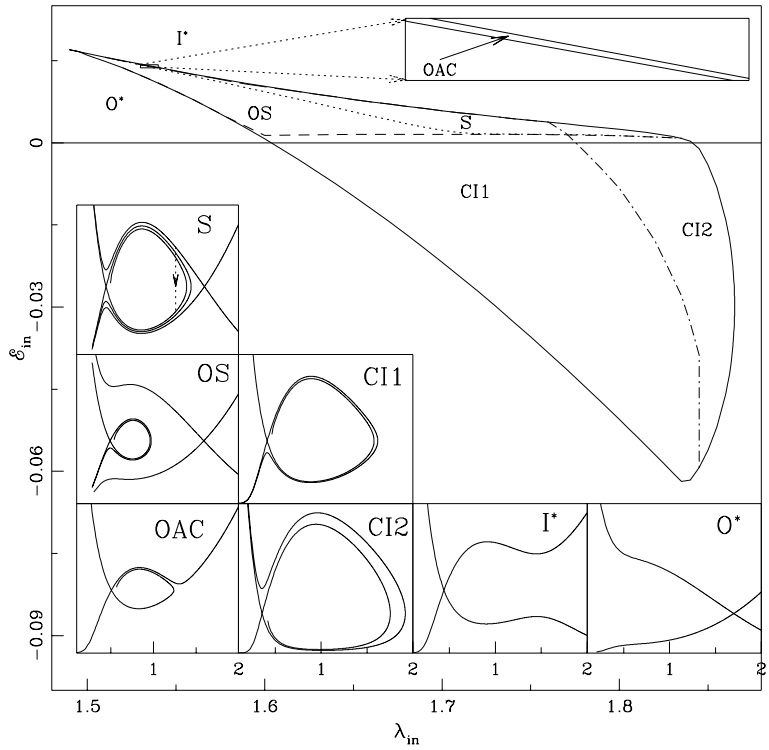

Figure 10. Division of the parameter space $\mathcal{E}_{in}$, λ_{in} (marked) for a viscosity parameter ($\alpha_\Pi = 0.01$) on the basis of the solution topologies shown in the boxes (marked). See text for details.

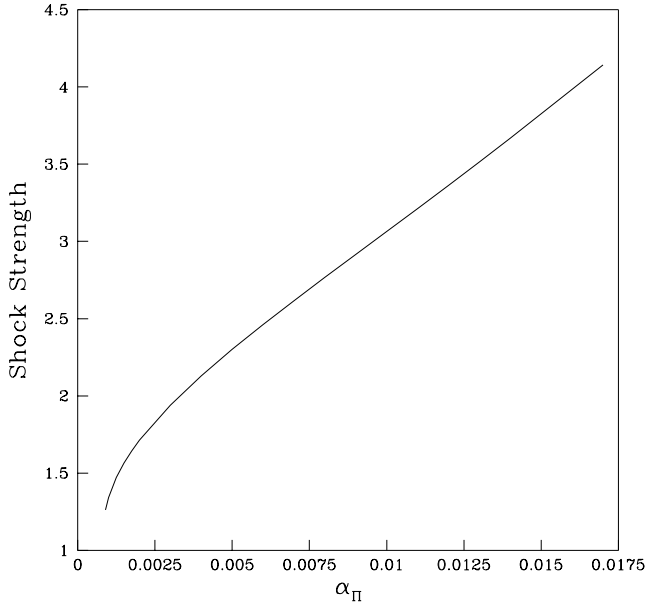

Figure 11. Variation of the ratio of the pre-shock to post-shock Mach numbers as a function of viscosity parameters for a fixed set of initial conditions ($x_{in} = 2.795$ and $\lambda_{in} = 1.65$). The shock disappears beyond the critical parameter $\alpha_\Pi \sim 0.017$.

box marked O*. An accretion flow solution with these parameters passes only through the outer sonic point before falling into the black hole (similar to a Bondi flow).

Since the strength of the shock determines the jump in temperature and density, it may be worthwhile to study the shock strength. We define this as the ratio of the pre-shock Mach number to the post-shock Mach number. As an example, in Fig. 11 we show the variation of the shock strength as a function of viscosity parameter α_Π. This figure is drawn for $x_{in} = 2.795$ and $\lambda_{in} = 1.65$. For the lower viscosity limit, the strength of the shock is weak. It increases smoothly with the gradual increase of viscosity and there is a cut-off at a critical viscosity limit where the shock disappears.

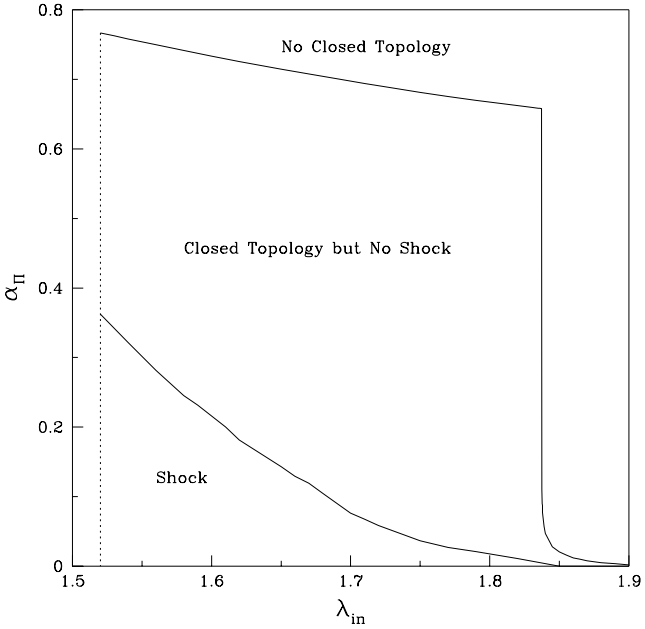

Figure 12. Critical viscosities separating standing from oscillating shocks and closed topologies from open topologies.

7 DEPENDENCE OF THE CRITICAL VISCOSITY PARAMETER

In our earlier discussion, we already hinted that there must be a critical viscosity parameter for which the flow topology must change its nature from an open topology to a closed topology. Here, we quantify the nature of this critical viscosity. Indeed, we find that there are in effect two critical viscosity parameters: one at the boundary which separates the closed topology from the open topology while the other splits the region of the closed topology in terms of whether shocks can form or not. Not surprisingly, these are dependent on the inflow parameter, and thus do not have universal values. Nevertheless, these are useful, since they give us insights into the cases in which shocks may be possible.

Fig. 12 shows the variation of the critical viscosity parameters with the angular momentum at the inner sonic point. Different regions are marked. We note that for higher viscosity parameters (α_Π), shocks are formed in the lower angular-momentum domain. As the angular momentum is increased, the shock disappears. This was also expected from our discussion of Fig. 1(c).

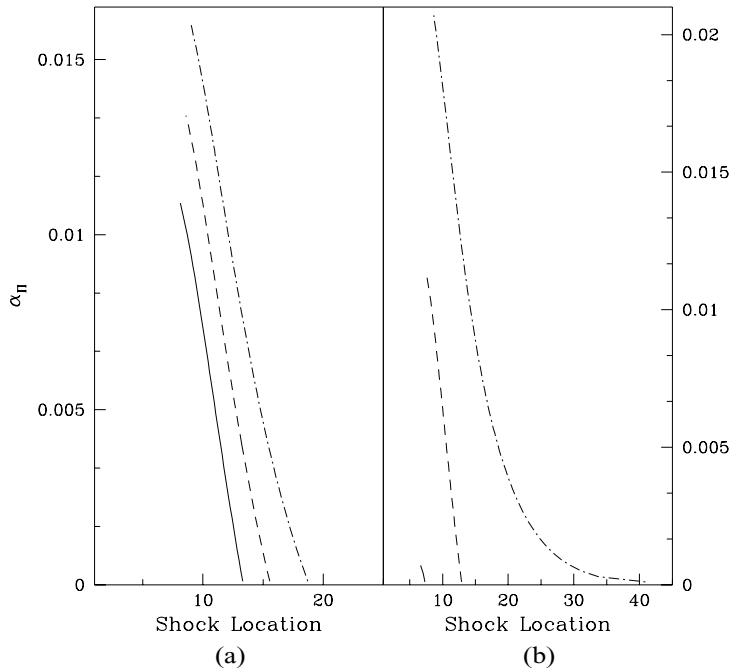

Figure 13. Variation of shock location with viscosity parameter and (a) inner sonic point and (b) specific angular momentum. The shock location always decreases with increase of viscosity until the critical viscosity parameter is reached, beyond which the shock ceases to exist.

8 DEPENDENCE OF THE SHOCK LOCATION ON VISCOSITY PARAMETER

In our study of shock properties, we have already mentioned that the shocks disappear when the viscosity is more than a critical value. In Figs 13(a) and (b) we show how the shock location depends on the viscosity parameter when the other two free parameters, i.e. the sonic point location ($x_{\rm in}$) and angular momentum ($\lambda_{\rm in}$), are kept fixed. In Fig. 13(a), the variation with the inner sonic point is shown when the angular momentum is kept fixed, while in Fig. 13(b), the variation with the angular momentum is shown, keeping the inner sonic point fixed. In all cases, the shock location is reduced with the increase in viscosity parameter till the critical viscosity parameter is reached, beyond which the shock ceases to exist. This is significant because in an accretion flow, when the viscosity is increased, the accretion rate is also increased and a black hole candidate goes from a spectrally hard to a spectrally soft state (CT95). Thus if the shock oscillation is indeed the cause of quasi-periodic oscillations (QPOs), then the frequency should increase with the accretion rate and finally as the shock ceases to exist, the QPOs also should disappear in softer states. Observation of such features could be used to verify if the shock oscillations may be the prime cause of the QPOs in black hole candidates.

9 CONCLUDING REMARKS

In this paper we have extended our earlier results of the study of shock formation to include the very difficult yet more realistic case of viscous polytropic flows. Some of the results have been touched upon in C96a but the new results in our work include a detailed study of the parameter space in which shocks form, even in the presence of viscosity. We found a large number of important results.

(i) There exist two critical viscosity parameters which separate the region of the parameter space into three parts: (1) in which the flow has a Bondi-type single sonic point; (2) in which there are three sonic points but no Rankine–Hugoniot relations are satisfied and (3) when the Rankine–Hugoniot relations are satisfied. These critical viscosity parameters decrease with the increase of the specific angular momentum of the flow at the inner sonic point.

(ii) At high viscosities, standing and oscillating shocks may form if the flow has very little angular momentum at the inner sonic point, while at low viscosities the situation is exactly the opposite. It is widely believed that accreting matter on galactic and extragalactic black holes could be of very low angular momentum, especially when the central compact object is accreting winds from a nearby star or stars. This brings out the possibility that shocks may be active ingredients of an accretion flow. Our results, with very plausible accretion flow models, indicate that standing and oscillating shocks are produced even for large viscosity parameters.

(iii) The shock location is reduced with enhancement of the viscosity parameter. This, coupled to earlier results (Chakrabarti & Manickam 2000) that the infall time is proportional to the period of quasi-periodic oscillation (QPO) of X-rays from black holes, implies that the QPO frequency should increase as the viscosity is increased. This is consistent with the observational findings that the QPO frequency is increased as the spectral slope softens, widely known to be due to an increase in viscosity and accretion rate.

One of the questions we have not addressed here is the stability properties of these shocks. A number of authors have pointed out that while the shocks are stable they should undergo oscillations, either radially, or vertically, or non-axisymmetrically (Molteni, Toth & Kuznetsov 1999; Gu & Foglizzo 2003). We anticipate that our shock solutions in viscous flows would suffer similar types of oscillations, especially when the viscosity is low. In particular, Gu & Foglizzo (2003) while studying shocks in inviscid, isothermal flows, found such instability and interpreted it as being due to cycles of acoustic waves between their corotation radius and the shock. In their interpretation this could be a form of Papaloizou–Pringle instability (Papaloizou & Pringle 1984) which is known to destabilize accretion tori when the angular momentum gradient is less than a certain value. If so, such an instability could disappear at high enough viscosity. This could have a bearing on the quasi-periodic oscillations of observed X-rays in galactic and extragalactic black hole candidates in that QPOs would cease to exist above a certain frequency. The interesting aspect is that these so-called ‘instabilities’ only cause oscillation of shocks and do not destroy the shock (Molteni et al. 1999).

ACKNOWLEDGMENTS

This work is partly supported by a project (Grant No. SP/S2/K-15/2001) funded by the Department of Science and Technology (DST), Government of India.

REFERENCES

Chakrabarti S. K., 1989a, MNRAS, 240, 7 (C89a)
Chakrabarti S. K., 1989b, ApJ, 347, 365 (C89b)
Chakrabarti S. K., 1990a, Theory of Transonic Astrophysical Flows. World Scientific, Singapore (C90a)
Chakrabarti S. K., 1990b, MNRAS, 243, 610 (C90b)
Chakrabarti S. K., 1996a, ApJ, 464, 664 (C96a)
Chakrabarti S. K., 1996b, MNRAS, 283, 325 (C96b)
Chakrabarti S. K., 1998, in Chakrabarti S. K., ed., Observational Evidence for Black Holes in the Universe. Kluwer, Dordrecht (C98)
Chakrabarti S. K., 1999, A&A, 351, 185
Chakrabarti S. K., Manickam S. G., 2000, ApJ, 531, L41

Chakrabarti S. K., Molteni D., 1993, ApJ, 417, 672
Chakrabarti S. K., Molteni D., 1995, MNRAS, 272, 80 (Paper I)
Chakrabarti S. K., Titarchuk L. G., 1995, ApJ, 455, 623 (CT95)
Chattopadhyay I., Chakrabarti S. K., 2002, MNRAS, 333, 454
Das S., Chattopadhyay I., Chakrabarti S. K., 2001, ApJ, 557, 983
Das S., Chakrabarti S. K., 2004, MNRAS, submitted
Gu W.-M., Foglizzo T., 2003, A&A, 409, 1
Holzer T. E., Axford W. I., 1970, ARA&A, 8, 31
Landau L. D., Lifshitz E. D., 1959, Fluid Mechanics. Pergamon, New York
Lanzafame G., Molteni D., Chakrabarti S. K., 1998, MNRAS, 299, 799 (Paper II)
Lu J. F., Yuan F., 1997, PASJ, 49, 525L
Matsumoto R., Kato S., Fukue J., Okazaki A. T, 1984, PASJ, 36, 7
Molteni D., Sponholz H., Chakrabarti S. K., 1996a, ApJ, 457, 805
Molteni D., Ryu D., Chakrabarti S. K., 1996b, ApJ, 470, 460
Molteni D., Toth G., Kuznetsov O. A., 1999, ApJ, 516, 411
Nobuta K., Hanawa T., 1994, PASJ, 46, 257
Paczynski B., Wiita P. J., 1980, A&A, 88, 23
Papaloizou J. C. B., Pringle J. E., 1984, MNRAS, 208, 721
Ryu D., Chakrabarti S. K., Molteni D., 1997, ApJ, 474, 378
Shakura N. I., Sunyaev R. A., 1973, A&A, 24, 337
Smith D. M., Heindl W. A., Markwardt C. B., Swank J. H., 2001, ApJ, 554, L41
Smith D. M., Heindl W. A., Swank J. H, 2002, ApJ, 569, 362
Yang R., Kafatos M., 1995, A&A, 295 238

This paper has been typeset from a TEX/LATEX file prepared by the author.